Optical measurements of morphology-to-functional parameters on electrical contacts of photovoltaic cells

Optical measurements of morphology-to-functional parameters on electrical contacts of photovoltaic cells

To cite this article before publication: Roberto Bellotti *et al* 2019 *Surf. Topogr.: Metrol. Prop.* in press https://doi.org/10.1088/2051-672X/ab370e

Optical measurements of morphology-to-functional parameters on electrical contacts of photovoltaic cells

Roberto Bellotti [(1)], Valentina Furin [(2)], Alessandro Marsura [(1)#], Gian Bartolo Picotto [(1)], Luigi Ribotta [(1)*]

[(1)] Istituto Nazionale di Ricerca Metrologica (INRiM), Strada delle Cacce 91, 10135, Torino, Italy

[(2)] Applied Materials Italia s.r.l., via Postumia Ovest 244, 31048, Treviso, Italy

[#]Present address: Via Vanizza 62, 31025, Santa Lucia di Piave, Italy

*Corresponding author: Luigi Ribotta

l.ribotta@inrim.it

Keywords: functional surfaces, morphology parameters, resistance measurements, printed electrical contacts, solar cells

Abstract

Traceable parameters for determining the relationship between texture, form, sizes and resistance behaviour of functional surfaces' features, such as screen-printed electrodes with grids of different design either on c-Si photovoltaic cells and on a ceramic substrate, are studied in this work. Test samples with electrodes of various sizes, suitable to study surface features in a wide measurement range, have been characterized by optical-confocal profilometry and by resistance measurements with dense data sampling. Quantitative measurements of these printed lines in terms of descriptors like the cross-section area and its variations along the segment, and of the top-profile roughness, scaling of roughness, and fractal dimension are presented and discussed either for photovoltaic cells and test structures. A good agreement between the resistance calculated from optical-based 3D morphology measurements and local resistance measurements on these electrodes is demonstrated.

1. Introduction

The characterization of engineered surfaces on highly-parallel manufacturing is a key point to enable quality control towards ever higher production volumes and at ever higher production speeds. This is why inline controls become a challenge, and the feasibility of correlating morphology to functional properties of engineered surfaces is of great importance today [1].

Solar cell manufacturers constantly increase efficiency (i) by printing narrow finger in order to limit the shading effects on the photoactive surface and (ii) by improving their metallization processes, trying simultaneously to reduce paste consumption for saving processing costs [2]. To date, the screen printing of electric front contacts has got very high throughput (one cell is printed in a few seconds), with expected further increments of the wafers per hour by the continuous improvement of manufacturing processes [3]. Double-printed front contact fingers on crystalline silicon (c-Si) are now made with narrower width, thus reducing shading losses on solar cell, compared to single printing configuration [4]. Thanks to such steps, it has been demonstrated 0.46 % absolute cell efficiency gain and up to a 10 % reduction in consumption of silver printing paste [2].

Screen printing is widely used for metallization of solar silicon cells in today's production, providing superior economic benefits, extendibility to multiple cell designs, and continuous improvements in terms of consumables and equipment [4]. Pasta suppliers have played a crucial role over the last ten years to ensure better cell performance at a lower dollar-per-watt cost, obtaining additional cost savings and improving cell efficiency. The metallic contact formation by screen printing is related to the composition of the paste, that influences the resistivity, and to the thermal process, that promotes the sintering of the metal with the silicon or, in the case of heterojunctions, with the transparent conductive oxide (TCO). Generally, each cell manufacturing process should be performed at a temperature equal or lower than that of the deposition of the amorphous layers that compose the emitter. For this reason, the metallization of heterojunctions for screen printing must be performed at a maximum temperature of 850 °C (firing); it is important to note that ohmic contact, metal conductivity, and aspect ratio (height/width ratio) of the grid depend on the properties of the used paste and from the printing process [5].

Therefore, it is a fundamental priority to study the optimal performance of the electric contact grid (formed by busbars and fingers) as a function of cell efficiency, that depends on functional parameters [6,7,8], such as the line resistance. Resistance measurements are slow to perform due to surface-probe contacts, while 3D topography parameters are significantly faster by non-contact optical measurements. Considering a real scenario where screen printed features rarely have an ideal rectangular shape, trapezoidal cross-sections are used for a more realistic modelling of the fingers [9]. Quantitative measurements of surface roughness/texture play a significant role in the analysis of engineered functional surfaces [10]. Roughness influences mechanical properties of materials, while texture determines the reliability and/or functionality of manufactured goods [11]. Alongside applications in mechanics, optics, electronics and precision micromechanics electronics, new and stringent measurement requirements are highlighted for texture analysis in the parallel manufacturing of functional surfaces. These measurement requirements have stimulated the extension of the normative regarding surface metrology. Measurement instruments, reference samples, parameters and curves feature in the roughness/texture are subjects of profile and areal parameters (ISO 4287 and ISO 25178 under development) [12,13], and of ISO 5436 (height parameters) [14] written standards, which take part of the geometrical product specifications (GPS) system.

Advanced technologies under development for reconstructing topography of large areas with good speed would make profit of a well-established panel of traceable parameters correlating morphology and functional properties of surfaces [15]. In this framework, test cases representing printed linear conductors (PLCs) are assumed for this study. Correlation between morphology and line resistance of fingers of PV cells and test structures is discussed with the aim of highlighting well-identified morphological parameters suited to printed conductors in solar cells production. In order to compare features of fingers printed on different supports, samples of PV standard cells on silicon, PV heterojunction bifacial cells and test structures with fingers of different width printed on a ceramic substrate, have been tested.

2. Materials and Methods

2.1 Instrumentations and set-ups

Interference microscopes make use of the so-called phase-shifting interferometry (PSI) and vertical scanning interferometry (VSI) techniques for areal surface topography measurements of smooth and rough surfaces. Among others, chromatic or intensity confocal are also powerful imaging methods for areal and profile surface measurements. Most of these imaging technologies are now available in instruments operating with complex algorithms and on-board metrology for the different methods, thus requiring a well-established procedure for the calibration of the instrument.

The instrument in use at INRiM is a Sensofar PLμ 2300 optical profiler, which allows for PSI, VSI, and intensity confocal imaging modes with objectives from 5X to 100X, and with a phase-grating displacement transducer coupled to the vertical axis and a piezo-resistive sensor inside the objective moving stage. The profilometer lies on a Halcyonics Micro 60 antivibration table, this last placed on a high-performance optical table with laminar flow isolator supports. *In-situ* calibration of the vertical axis of the instrument is performed by an interferometer set-up, while magnification (pixel size, squareness) of the objectives is determined by 2D gratings calibrated by an optical diffractometer.

3D images of fingers, taken with a 50X objective, are approximately 250 μm x 250 μm side, therefore reconstructing surface morphology of up to a few millimeters segment requires stitching of at least 10 images. Mosaic of images is provided by the profiler itself, whereas image analysis is based on metrological software tools [16, 17], by which the top longitudinal profile and cross-section area (CSA) of fingers are analyzed in terms of roughness and waviness parameters.

The PV cells are placed on a universal substrate sample fixture (USSF) [18], a tool designed for multi-purpose inspection of large-area topography and functional performance measurements on thin and flexible substrates. This set-up incorporates a universal base plate for permanent installation, kinematic locators and semi-disposable substrate clamps, designed to transfer an absolute coordinate system with a lateral repeatability of few tens of μm between multiple probes/tools. The USSF is used in this study to enable repeatable collocation of topography and resistance measurements.

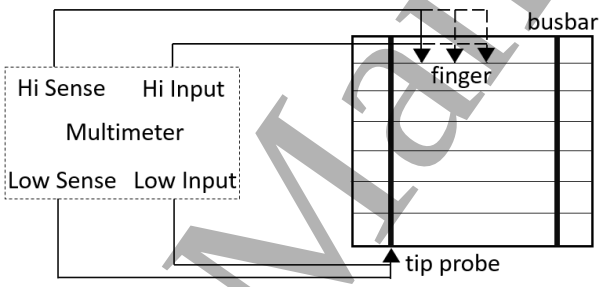

Figure 1 Global connection locations of the 4-wire like resistance measurements set-up.

Resistance measurements made use of an Agilent Keysight 3458A multimeter. As sketched in Figure 1, there is one metallic tip probe contacting a busbar and another one contacting a finger, each tip probe connected to current-carrying and/or voltage-sensing terminals of the multimeter. In 4-wire resistance method, a known current is provided through the unknown resistance being measured by the voltage drop across it and by the feed current [19]. This set-up allows more accurate measurements for low resistance values, because current and voltage electrodes are separated minimizing the effect of lead resistance. Values of resistance, by a fixed reference electrode connected to a busbar and a working electrode moving along the finger, are taken at given positions along the segment to be measured. The moving probe is mounted on the objective revolver of the profilometer, by which it is driven at contact with the finger. The electrode approaches the surface until an early electrical contact is achieved by the multimeter readings; then, the resistance is measured by loading of about 0.15 N the retractable elastic tip to get a good contact. A tip-sample elastic deformation of about 45 nm is calculated with the applied load [6,20,21]. With our 4-wire like set-up, the resistance of connecting wires is minimized but the contact resistance between electrodes (metallic tips) and printed busbars or fingers remains and contributes by a constant term.

2.2 Test cases description

Different samples are studied, in particular test structures with PLC on alumina substrate, p-type standard c-Si solar cells, and n-type heterojunction bifacial cells. In the following are reported the results achieved

with samples from these lots. It should be noted that these results well represent the other samples of the same lot.

The grid of these specimens has a different design, that led to slightly change of the equivalent circuit of parallel fingers (section 3.1.2).

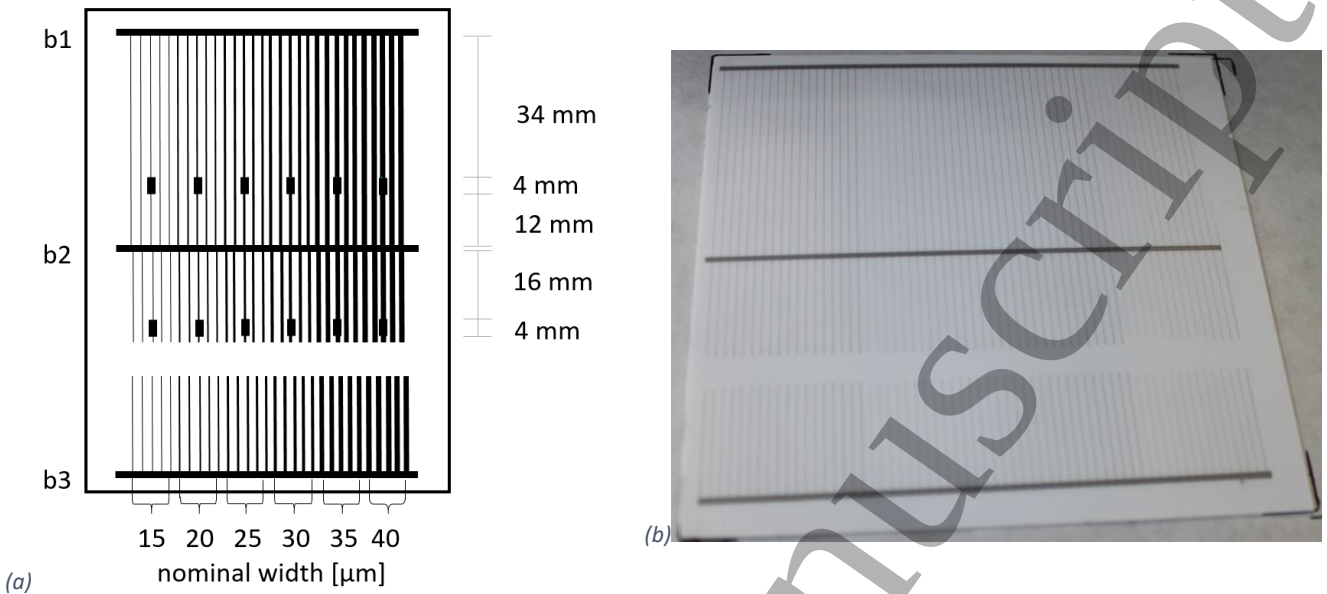

Figure 2 Sketch (a) and photograph (b) of the test structure on a ceramic plate. The grid has open and continuous fingers in groups of different nominal width (from 15 µm to 40 µm) connected to three busbars. Selected segments 4 mm long are those in bold, from the third finger of each group.

Test structures with busbars and fingers of various sizes (width and thickness) on a ceramic substrate of 150 mm x 150 mm x 0.5 mm have been provided by Applied Materials Italia, that designed the test pattern layout for screens manufacturing and printed it on substrates. Their grid's design (Figure 2) drawn by 3 busbars and 60 fingers with nominal widths ranging from 15 µm up to 40 µm. As in the layout of all solar cells, fingers are connected to the grid between busbar 1 and busbar 2, while between busbar 2 and busbar 3 are deliberately open; in this way, shorter fingers are connected only to one busbar with the aim of avoiding the influence of parallel fingers on resistance measurements. These fingers are named as "open fingers", while those connected both sides to the grid are named as "continuous fingers".

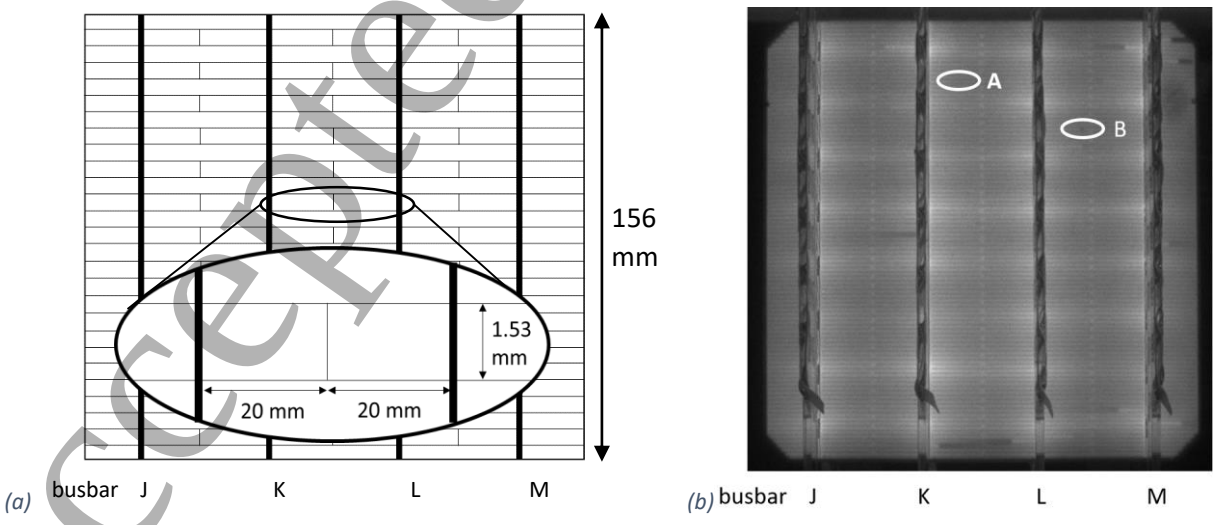

Figure 3 (a) Not to scale sketch and (b) electroluminescence image of a p-type standard c-Si solar cell.

In Figure 3 (a) is given the sketch of a p-type standard c-Si solar cell (156 mm x 156 mm x 0.18 mm), that takes part of a lot of 20 cells having a grid design with fingers in pairs between busbars, and pairs are connected to each other at their mid-length. Electrical contacts on crystalline silicon cells are obtained by single print passing a Heraeus 9642B paste on a stencil with 101 fingers. The contacts thus printed are undertaken to a firing process for 1 minute at the temperature of 850 °C. Figure 3 (b) shows an electroluminescence (EL) image taken at Applied Materials Italia by using an infrared camera with a resolution of 320 pixels x 240 pixels; the EL image is obtained by fixing the voltage and varying the current through the cell.

This lot of standard c-Si PV cells have been manufactured and tested by Applied Materials Italia providing a statistical study of thickness, width, aspect ratio and roughness of their fingers. Then, measurement runs have been performed at INRiM to investigate morphology and resistance of a number of finger segments, identified by the capital letters in white in the EL image. It is worth noting that local change of contrast in the EL image may identify the presence of local defects.

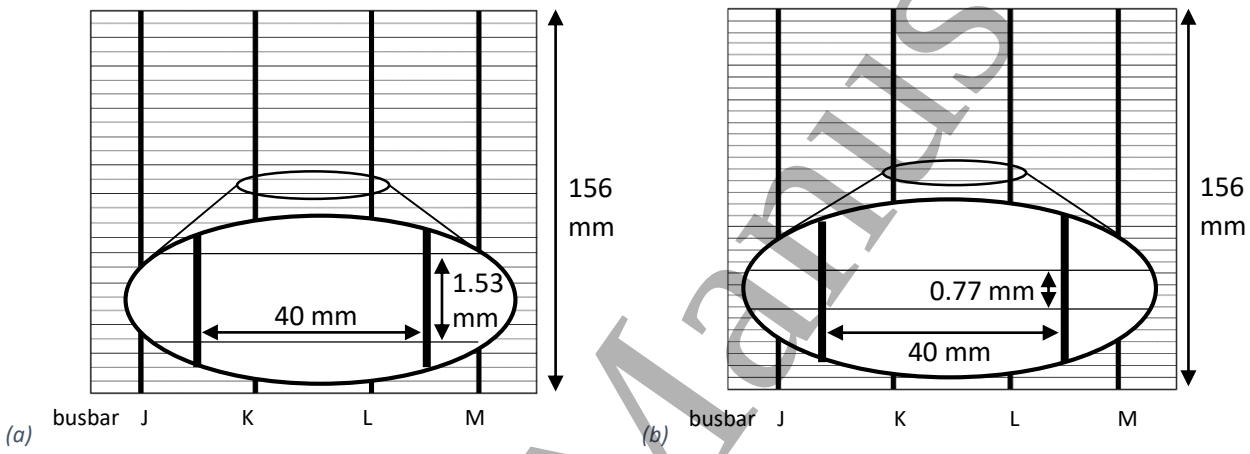

Figure 4 (a) Front-side and (b) back-side not to scale design of the grid of a n-type heterojunction bifacial cell.

Figure 4 shows the grids of the two sides of a n-type heterojunction bifacial cell (156 mm x 156 mm x 0.18 mm). The front-side grid has 4 busbars and 101 fingers, while the back-side has 200 fingers. The electrical contacts are screen printed on both sides, by means of an automatic screen printer using a wire diameter of 16 µm and a screen with 325 mesh; the printing direction is parallel to fingers with 200 mm·sec^{-1} printing speed. After that, they have undergone a curing process of less than 800 °C for 3 seconds, using an oven by Applied Materials Italia. This new type of solar cells will be used in solar module, where the front side is directly exposed to the sun, while the back side requires more fingers because it collects the radiation backscattered, *e.g.* from a wall. Thanks to the collection of the scattered light, this technology enhances the efficiency of about 10 % compared to current technologies, where this diffused radiation is not collected.

3. Results and Discussion

3.1 Surface-function models

3.1.1 Topographic analysis

Previous measurements of PLC's morphology [22] by optical non-contact have shown a good agreement of results with those by stylus profiling, that is the classical reference technique for topography and roughness data in the microscale of touchable surfaces. This allows to perform faster and robust

measurements using non-contact instruments, thus reducing analysis time permitting in the future to the manufacturing industries to perform next-to-line control.

In order to determine top roughness and sizes (height and width) of screen-printed fingers, high resolution 3D surface topography (about 3 100 pixels/mm) is reconstructed using an intensity confocal profiler with a 50X objective. Figure 5 shows a 3D view of a 5 mm finger segment reconstructed by the stitching of 25 images (with an overlapping area between each image of 20 %) using the own control software (SensoScan 2300) of the instrument. 3D images of segments from 2 mm to 5 mm lengths with about 3 100 pixels/mm are taken and compared to achieve consistent texture data (roughness and waviness) at different evaluation lengths. Texture components and roughness parameters are extracted from the longitudinal profile of the finger, while shape and sizes from their cross-sections.

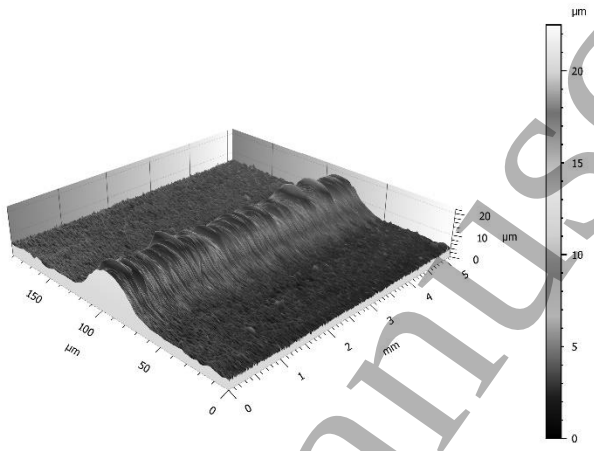

Figure 5 3D view of a 4 mm length of a finger on the back side of a bifacial cell.

The mean height of fingers is extracted from the cross-section profile at each pixel of the segment length, by using a step-height software tool [6]. Assuming a trapezoidal-based model of the finger cross-section area [9], a new morphological descriptor CSA is identified to represent the morphology of fingers, and therefore also the grid printed quality. The isosceles trapezoid approximation is fairly well representative of the finger section as reconstructed by optical profiling. Furthermore, it helps to reduce errors from spikes and local optical effects at finger sides. In equation (1) is reported the CSA at the i-pixel of the segment length, where W_f is the base width, t_f is the thickness and θ_f is the side slope (Figure 6).

$$CSA_i = \left(W_f - \frac{t_f}{tan\,\theta_f}\right) t_f \qquad (1)$$

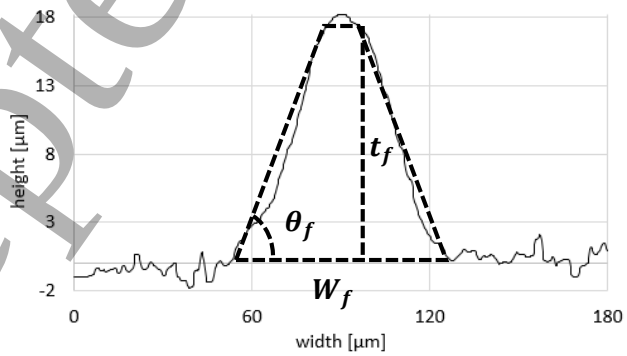

Figure 6 Trapezoidal shape approximation of the cross-section area.

The aim of this study is to correlate morphological features to the resistance of the finger segment, namely to underpin topography-based calculated resistances from direct resistance measurements. The resistance can be calculated from the sum of the resistance R_i of the elementary segment length dl by the second

Ohm's law in (2), where CSA_i is the cross-section area at the i-pixel and ρ_f is the gridline resistivity, which is assumed of $2.7 \cdot 10^{-8}$ Ω·m in accordance to available data for silver paste [9, 23].

$$R_i = \rho_f \frac{dl}{CSA_i} \qquad (2)$$

3.1.2 Resistance analysis

An equivalent electrical circuit of the grid layout is needed to quantitatively analyse the results of resistance measurements along the segment of a finger. The model reported in [22] is valid for the specific design of the p-type standard c-Si solar cell, while it has been slightly modified for the layout of the ceramic test structure (Figure 2) and for the bifacial cell (Figure 4). This is due to the fact that in the cells of Figure 3 the fingers pairs are interconnected at their mid length.

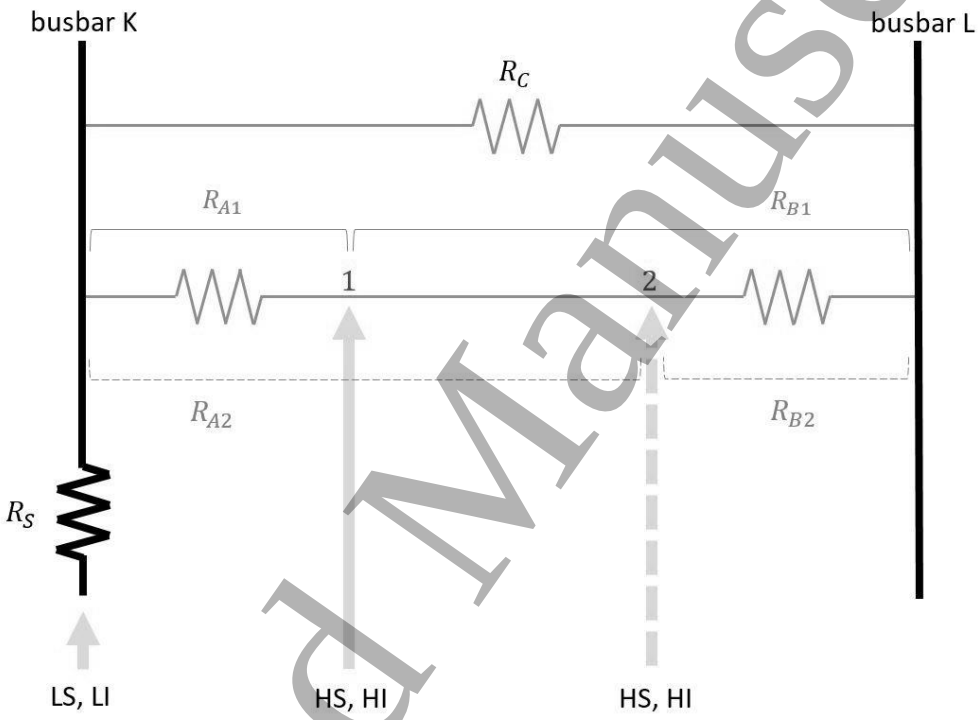

Figure 7 Sketch of the equivalent circuit assumed for grids of classical layout, e.g., bifacial cells and ceramic test structures (continuous fingers).

A simplified equivalent circuit of the 4-wire like resistance measurements of cells with classical grid design is sketched in Figure 7, where the Low Sense (LS) and Low Input (LI) reference electrodes are connected to each other at the tip pointing the busbar K, while the Hi Sense (HS) and Hi Input (HI) electrodes are connected to the tip moving along the finger segment to be measured.

The resistance R_A in the equivalent circuit in Figure 7 represents the resistance of the segment L_A (between the reference probe on the busbar K and the sampling point of the moving probe along the segment to be measured), and R_B the resistance of the complementary segment L_B toward the busbar segment L (note that the finger length is the sum of L_A and L_B). R_S is the resistance in series mostly due to the contact resistance of the tip probes with the grid, which is still present in our measurement set-up. R_C is the resistance in parallel by all the fingers connecting busbars K and L and the remaining part of the grid. Minor contributions are estimated from the parallel of fingers connecting the busbars J-K and L-M (Figure 4) in parallel with a busbar (the larger the width, the lower the resistance of lines having same thicknesses), and from the resistance of the semiconductor substrate. This last comes from an initial estimation based on the

available PV semiconductor data, further strengthen by comparing resistance measurements based on the simplified circuit either on fingers on PV cells and on test structures on alumina.

The resistance R_1 measured at a given point 1 of the finger segment (Figure 7) is described in equation (3), and is given by the parallel of the resistance R_{A1} of the segment L_{A1} and the sum of the resistance of the complementary segment R_{B1} and the parallel resistance R_C, plus the contact resistance R_S. In a similar way, the resistance measured at the point 2 of the finger segment is described in equation (3) as R_2.

$$R_1 = R_S + \frac{R_{A1} \cdot (R_{B1}+R_C)}{R_{A1}+R_{B1}+R_C} \qquad R_2 = R_S + \frac{R_{A2} \cdot (R_{B2}+R_C)}{R_{A2}+R_{B2}+R_C} \qquad (3)$$

From equation (3) the terms without the influence of the grid parallel and the series resistance (R_{A1} and R_{2A}) are extracted, and the resistance of the segment $1-2$ is calculated by the difference $R = R_{A2} - R_{A1}$, named in the text as "measured resistance". As a first approximation of equations (3), the mean resistance of a finger segment is assumed equal to that of other segments of the same length. This assumption does not prevent to correlate the measured resistance with the "calculated resistance", that is the line resistance calculated as the sum of the elementary resistances in equation (2) along the sampled segment.

3.2 Morphological parameters

Surface characteristics influence the behavior of the material, and they strongly depend on the chemical and physical mechanisms involved in the fabrication process. Morphological parameters are studied in order to describe the morphology of the top of the finger and quickly identify the goodness of a screen-printed grid. Good printing quality includes that all structures are printed as planned, and so fingers must have homogenous thickness and width, and do not present damages or interruptions.

3.2.1 Top-roughness profile

3D morphologies reconstructed from stitched images are undertaken to the filling of non-measured points by a smooth shape calculated from the neighbors, and to the removal of the mean slope of the entire image. A first analysis consists in extracting the central profile along the longitudinal top surface of the finger and calculating its spatial frequency spectrum. As expected, components of the same wavelength may easily be identified by the spectrum of top profile and of the CSA profile, which may reach in agreement the same information.

2D profiles of the finger top are evaluated in terms of classical roughness parameters [8,24] and of the fractal dimension. The average roughness R_a is the profile deviation from the mean line of the finger top roughness profile calculated along L, that is the sampling length that corresponds to the high-pass filter cut-off value λ_C applied to the finger primary profile. However, R_a is not sufficient to completely define the morphological characteristics of the surface, as profiles with different trends may have the same arithmetic mean deviation. For this reason, we study the root-mean-square (rms) roughness R_q, that is more sensitive to the presence of peaks, also identify by the maximum height of the roughness profile R_z.

In addition, R_q is calculated at different cut-off lengths L up to the total profile length of the segment analyzed, as the rms roughness scales by $R_q \propto L^{\propto}$ with the sampling length L, namely at shorter wavelengths. As shown in Figure 8 (a, b) for an open finger on the test pattern on alumina, the scaling factor α is given by the slope of the log-log plot of R_q at short cut-off length L. Then, R_q smoothly increases at longer wavelengths. The parameter α permits to quickly identify the trend of the rms roughness, namely the range of dominant wavelengths of texture at short and mid-scale lengths.

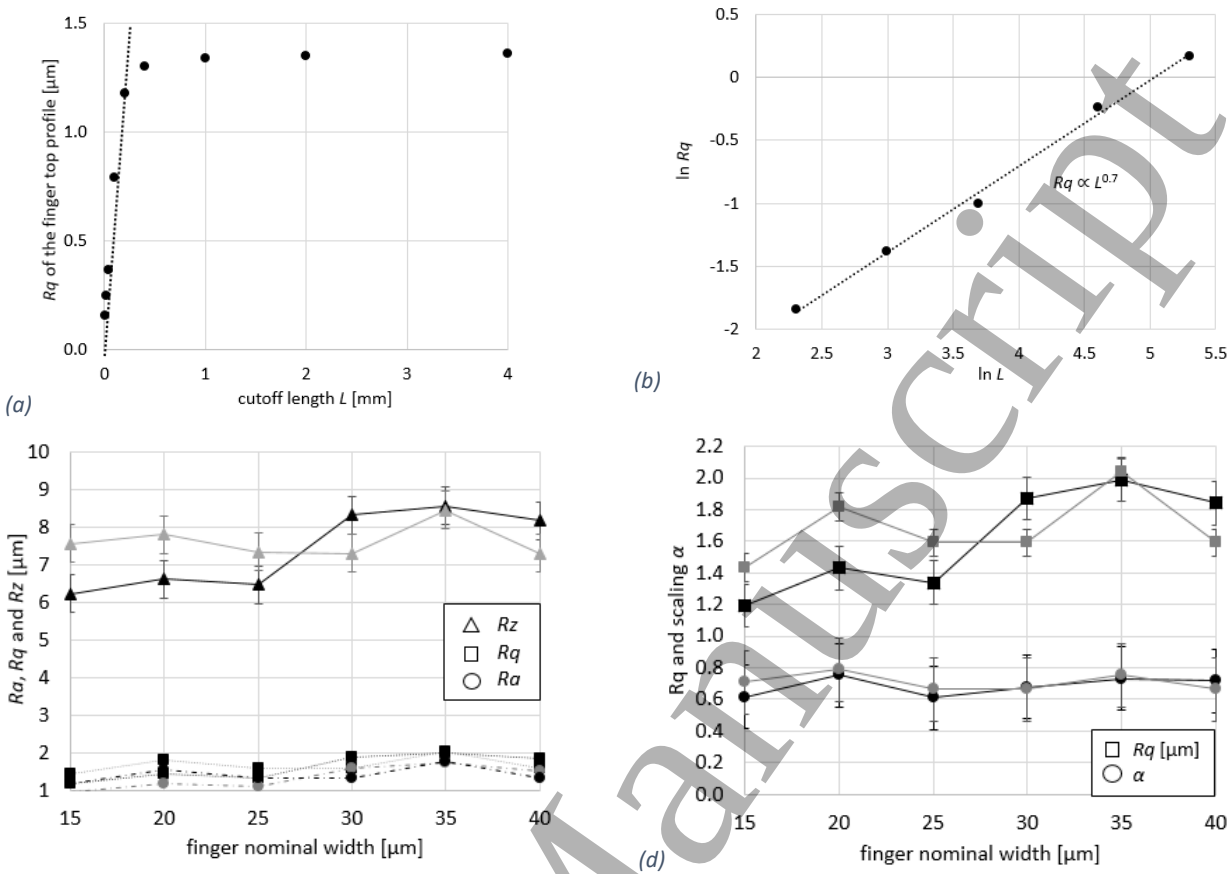

Figure 8 (a) Rq at different cutoff lengths L of the top profile of an open finger with nominal width 35 µm on the ceramic substrate. The dashed line represents the regression line at short cutoff lengths.
(b) ln(Rq) vs ln (L) plot calculated up to 0.4 mm of the cutoff length on an open finger with nominal width 35 µm on the ceramic substrate. The slope represents the Rq scaling.
(c) Ra, Rq and Rz of the finger top at segments 4 mm long on ceramic substrate.
(d) Rq and its scaling vs nominal width of fingers on ceramic substrate.
The error bars refer to expanded uncertainty, and the bold line ——refers to continuous fingers, while the grey line —— refers to open fingers.

Figure 8 (c) shows a comparison between roughness parameters of continuous and open fingers on test pattern on alumina, and it should be noticed that they do not change in a significant way between fingers of different nominal width. Minor variations of the roughness parameters may reflect local changes between the observed segment, not always representative of the full grid. Meanwhile, screen-printing technology does not make evidence of roughness-related issues when printing narrow fingers down to a few tens of micrometers. The roughness parameters R_z, R_a and R_q in Figure 11 (c) and (d) are calculated for an evaluation length of 4 mm and a cut-off length L = 0.8 mm [25]. Figure 8 (d) compares R_q and scaling α as calculated for open and continuous fingers, and it can be seen the same variation trend. The error bars in these plots refer to the estimated relative expanded uncertainty of roughness parameters, that is of 3 % for R_a and R_q, and of 5 % for R_z.

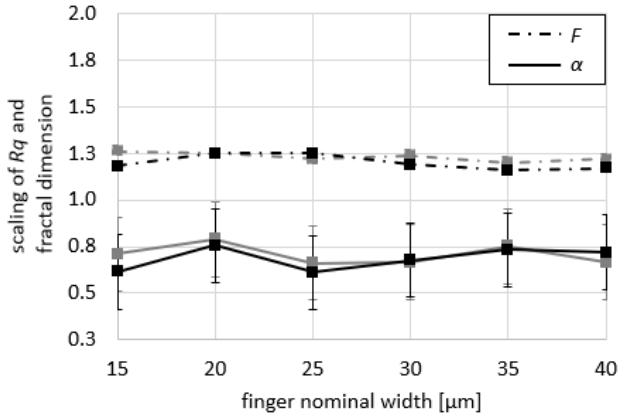

Figure 9 Scaling of Rq and fractal dimension vs. nominal width of continuous fingers on the ceramic test pattern. The error bars refer to expanded uncertainty, and the black line ——— refers to fingers connected to the grid, while the grey line ——— refers to open fingers.

In order to better understand texture and morphology aspects with high precision and low computational time, another parameter studied is the fractal dimension F of the finger top-profile. This non-dimensional parameter relates to complexity and self-affinity of surfaces, stating that the surface can be divided in subunits that exactly or statistically resembles the whole structure. A small fractal dimension value corresponds to a locally smooth surface structure, while a larger value of fractal dimension corresponds to a rougher morphology [26]. As demonstrated in Figure 9 the fractal dimension F and the roughness scaling factor α values agree quite well with their relationship given by $\alpha \sim 2 - F$, or otherwise by the rms method $R_q \propto L^{2-F}$ [27].

Table 1 shows roughness and fractal dimensions in bifacial cells and on the flawless sampling positions of the p-type standard c-Si cell, and in general it can be stated that defectless fingers have α values of about 0.8, F values of about 1.2 and R_q values of about 3 µm. For defected finger, it should be noted that all values are greater compared to those of flawless fingers. Table 1 gives also the wavelength of a common main component of top profile, by which a better insight of the printing process is expected. A principal wavelength component of the finger texture of about 120 µm is calculated for the test pattern on alumina, while the screen print mesh size is of about 140 µm for bifacial and standard cells, and it is higher for defected fingers.

Table 1 Rq (at λ_c 1 mm), scaling of Rq and fractal dimension F for fingers on ceramic substrate, on a central finger on front and back side of the n-type heterojunction bifacial cell, and on a flawless (position A) and defected (position B) finger segments of the p-type c-Si cell of standard design.

test cases	***test pattern on alumina***		***heterojunction cell***		***standard c-Si cell***	
segment			*front side*	*back side*	*A*	*B*
nominal width [µm]	*30*	*35*	*32*		*50*	
R_q [µm]	1.59	2.04	2.89	3.20	3.02	3.46
scaling α (st. dev.) of R_q	0.62 (0.04)	0.70 (0.05)	0.98 (0.05)	0.87 (0.04)	0.85 (0.05)	1.11 (0.06)
fractal dimension F	1.24	1.20	1.14	1.31	1.20	1.43
wavelength of a common main component of top profiles [µm]	~ 120		~ 140		~ 140	~ 200

An extended analysis of morphological parameters (width, thickness, top-roughness and aspect ratio) is reported in Table 2, together with their experimental standard deviation. Table 2 gives evidence of a good agreement of independent results, performed by Applied Materials Italia in five cells in 56 areas and by INRiM in five areas of one cell, including also segments with possible local defects, on the same lot of p-type standard c-Si cells. It is worth noting that a satisfactory (acceptable) value of aspect ratio (height/width ratio of the finger), a topic issue to have good conductivity and reduce shadow losses on c-Si cells, is achieved [28].

Table 2 Comparison of top roughness and mean sizes of fingers by measurements at INRiM (1 cell) and Applied Materials Italia (5 cells) performed on the same lot of p-type standard c-Si cells. The values in brackets refer to standard deviation.

	INRiM	Applied Materials Italia
number of sampled fingers	*5*	*56*
mean width [µm]	48.6 (6.7)	43.4 (2.3)
mean thickness [µm]	11.6 (3.8)	13.0
aspect ratio [%]	23.8 (0.4)	29.5
R_a [µm]	1.8 (0.4)	1.4
R_z [µm]	7.4 (1.1)	6.7
R_q [µm]	2.1 (0.4)	-

3.2.2 Cross-section area profile

The local values of the cross-section area along the segment of a finger are assumed to form a 2D profile of a quantity called CSA over the length l of the segment. Again, a trapezoidal shape of the cross-section area is assumed as given in the equation (1), and sizes and slopes of the trapezoid are determined at each pixel of the 3D reconstructed finger segment by using the "ISO 5436" tool of SPIP.

Waviness parameters provide a consistent way to analyze the profile of the CSA along the finger segment. The subscript A is used in the following to indicate the parameters dealing with the cross-section area. A cut-off value λ_f of 0.25 mm, larger than the dominant wavelength of finger top profile, is assumed. The first parameter studied is the total height of cross-section area profile $W_A t$. The larger the $W_A t$, the larger is the difference between the maximum and minimum values of the CSA; if this value is high, it quickly allows to understand the presence of defects or bottlenecks in the finger (and so the quality of the printing process).

Besides, the skewness $W_A sk$, that relies on the symmetry of the waviness profile respect to the mean line of the cross-section area, and the kurtosis $W_A ku$, that measure the sharpness of the waviness CSA profile, are calculated and given in Table 3.

For electric grids applications, it is preferable to have $W_A sk > 0$, because this indicates that few valleys are present in the CSA profile, and so there are not bottleckness and/or interruptions. Furthermore, $W_A sk > 0$ gives an idea of the segment resistance, that is low if the finger is homogeneous.

For what concern $W_A ku$, this value is critical if is < 3 (because there is a great data variability compared to the average value), while if it is equal or greater than 3 almost all data are around the mean waviness value, so the peaks and valleys are very sharp [29].

Table 3 Cross-section area profile waviness parameters for fingers on ceramic substrate, on a central finger on front and back side of the n-type heterojunction bifacial cell, and on a flawless (position A) and defected (position B) finger segments of the p-type c-Si cell of standard design.

test cases	***test pattern on alumina***		***heterojunction cell***		***standard c-Si cell***	
segment			*front side*	*back side*	*A*	*B*
nominal width [μm]	*30*	*35*	*32*		*50*	
$W_A t$ [µm²]	13.8	9.7	13.5	9.7	10.7	14.7
$W_A sk$	0.7	0.4	1.7	0.3	0.1	0.1
$W_A ku$	5.3	3.0	5.4	1.8	2.9	2.6

Table 3 compare CSA waviness values for the test cases studied, and it can be noticed that the mean value of $W_A t$ is about 12 µm². The CSA waviness skewness is close to 0 except for the front-side of the heterojunction cell, which show also high values of CSA (Table 3), CSA waviness skewness and CSA waviness kurtosis. $W_A ku$ is greater than 3 in all cases, except for the standard c-Si cell.

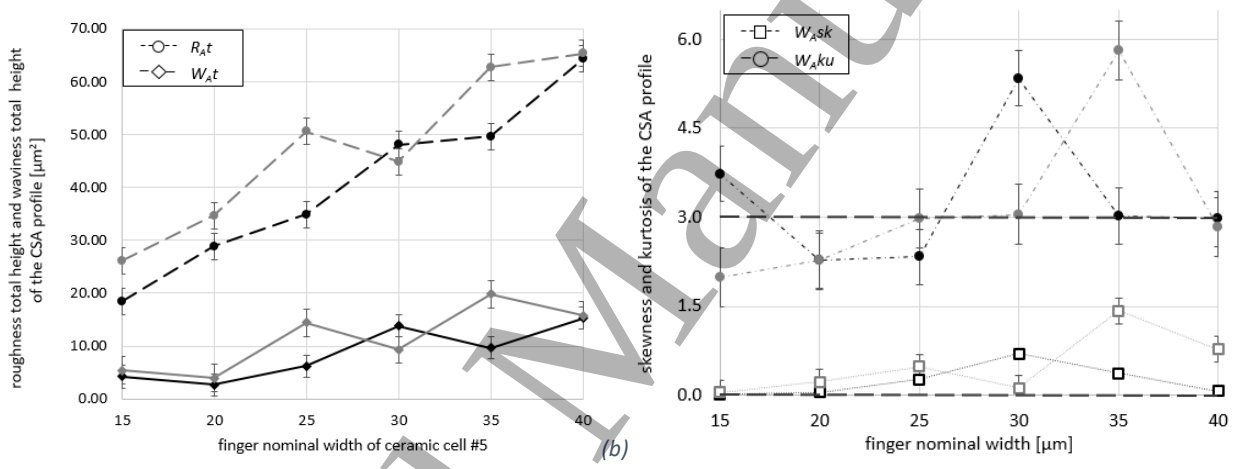

Figure 10 Parameters of the CSA profile of fingers on ceramic substrate: (a) roughness and waviness total height $R_A t$, $W_A t$; (b) skewness and kurtosis of waviness $W_A sk$, $W_A ku$. Note that thick dashed lines in (b) are made for the mean values of $W_A sk$ and $W_A ku$. The error bars refer to standard deviation, and the black line ——— refers to fingers connected to the grid, while the grey line ——— refers to open fingers.

Figure 10 compare waviness parameters of CSA of fingers on alumina substrate, showing $W_A t$ ranging from about 5 µm² to 20 µm², $W_A sk$ always with positive values indicating the presence of more peaks than valleys in the waviness profile, and $W_A ku$ minor than 3 for thinner fingers. In general, it may be noticed that the $W_A t$ and $W_A ku$ values for nominal widths of 15 µm and 20 µm differs from that of higher nominal widths, underlying the inhomogeneities present in the thinner fingers. Furthermore, Figure 10 (a) shows that the roughness total height of the CSA profile $R_A t$ and the waviness total height of the CSA profile $W_A t$ have the same trend.

3.3 Experimental results

3.3.1 Morphology by 3D optical imaging

3D morphology of fingers is reconstructed by using a Sensofar PLμ 2300 optical profiler operating in confocal mode, and by image stitching driven by the instrument. These images, processed using SPIP soft tool [17], are first undertaken to the interpolation of non-measured points by the mean calculated from the neighbors, and to the levelling by removal of the mean slope of the entire image. Subsequently, local variations of the cross-section of fingers are determined in terms of the mean height, top and bottom width by the 3D morphology, as reconstructed at each longitudinal pixel of the imaged segment. These local sizes are calculated by using the ISO 5436 software tool of SPIP [17].

A relative expanded uncertainty of about 15 % is estimated for the mean CSA of defectless segments reconstructed by 3D optical confocal imaging. Main contributions each of up to about 5 % relative standard uncertainty of the CSA come from the finger sizes (thickness, width and slope) and from the reconstruction errors due to void pixels, which may cause a somewhat large deviations of the local area. In addition, a mean CSA repeatability of about 2 % relative standard uncertainty by independent measurement runs, and minor contributions due to reference plane noise and levelling effects, are included in the budget as well.

Table 4 Thickness and CSA of the reconstructed segment of fingers on ceramic substrate, on a central finger on front and back side of the n-type heterojunction bifacial cell, and on a flawless (position A) and defected (position B) finger segments of the p-type c-Si cell of standard design. The values in brackets refer to standard deviation of sizes along the segment.

test cases	***test pattern on alumina***		***heterojunction cell***		***standard c-Si cell***	
segment			*front side*	*back side*	*A*	*B*
nominal width [μm]	*30*	*35*	*32*		*50*	
thickness [μm]	12.8 (1.5)	14.8 (1.8)	15.7 (3.1)	16.5 (4.3)	12.3 (3.2)	9.4 (4.3)
CSA [μm^2]	359 (49)	493 (72)	581 (129)	553 (129)	433 (77)	416 (177)

In Table 4 are reported thickness and CSA determined from the 3D images of segments on alumina test structure, on a standard c-Si cell and on the two sides of the bifacial cells. A larger standard deviation of values is visible for segments presenting local interruptions or significant variations of local sizes (segment B), which are also observed in the following by somewhat larger roughness parameters of the segment top profile. Thickness is up to about 15 μm, while the calculated CSA ranges from about 350 μm^2 to 600 μm^2. It is worth noting that sizes of segments on cells and test structures of the same lots are well represented by those in Table 4.

As a whole, a number of fingers identified from the EL image of the p-type standard PV c-Si cell have shown changes of up 5 % of the mean width and thickness at the various positions. Local variations of sizes may depend on screen printing parameters and chemical-physical features of the finger paste [30], and to a less extent on the silicon substrate.

Some differences on sizes (section 3.3.1) and texture (section 3.2) between fingers on test structure on alumina and PV cells with bifacial and standard design are outlined from the study; it is worth noting that those on alumina have been printed as a test structure, while bifacial and standard PV cells are printed in a manufacturing line, and so morphological characteristics of their fingers represent those of cells market available.

3.3.2 Resistance measurements

Resistance measurements are performed with the 4-wire-like set-up by dense data sampling on the same segment length previously imaged by the optical profilometer.

As mentioned above, the grid layout printed on alumina is created in order to avoid the influence of the semiconductor and of the parallel fingers in the resistance measurement of selected segments. With open fingers, the resistance increases linearly with the length as the parallel fingers do not contribute at all. In the open finger with nominal width of 25 µm (Figure 11), a slope of about 0.08 Ω·mm^{-1} is obtained by a linear regression of the resistance, as measured at steps of 0.2 mm along the segment of 4 mm length. The constant term comes from the segment representing the initial offset between the two probes and from the probe finger contact resistance. A resistance of 0.32 Ω is achieved with the 4 mm length segment.

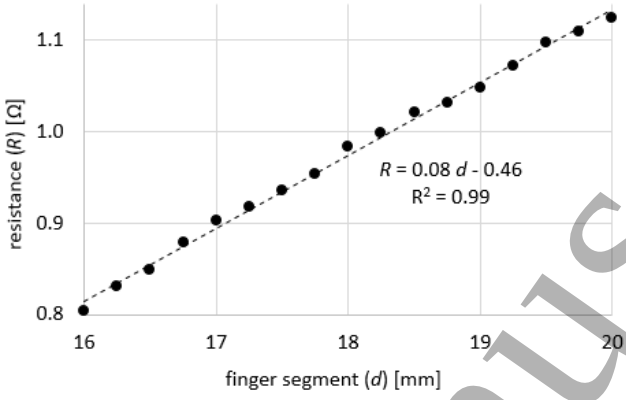

Figure 11 Resistances measured on a 4 mm segment length finger with nominal width of 25 µm in ceramic substrate.

Meanwhile, by assuming a resistivity value $\rho_f = 2.8 \cdot 10^{-8}$ Ω·m for the silver paste, the resistance calculated according to the sum of local resistances in equation (2) by the reconstructed 3D morphology of this open segment results of 0.31 Ω. A 3 % slightly higher resistivity than nominal value ($2.7 \cdot 10^{-8}$ Ω·m) best matches calculated and measured resistance for alumina test patterns, and this small increment of resistivity is possibly due to the difference in curing of the grid of these test structures compared to standard inline process. As is shown in Figure 12 (a), in open fingers on alumina the measured resistance differs by less than 10 % from that calculated from topography, while this agreement decreases for narrower fingers, due to the homogeneity issue in the printing process, as can be noticed in the photograph of the test structure (see Figure 2 (b)).

The resistance of segments of fingers with standard layout, *i.e.*, connected to the grid, is determined by the equation (3) and the equivalent circuit in Figure 7. Figure 12 (b) shows the trend between the resistance calculated either from the 3D reconstructed morphology and from nominal sizes of fingers, and the resistance of the segment. It is worth noting that for continuous fingers on alumina the agreement between calculated and measured resistance is at minimum 20 %, and as for open fingers this agreement decrease for narrower fingers (Table 5 and Figure 12 (b)). Furthermore, one can observe the presence of a shift between the measured and calculated resistances. Among others, these test patterns on alumina are made of fingers of different width, and may somewhat suffer from the approximation of the equivalence of segments of the same length, while in bifacial and c-Si p-type cells this evaluation is simpler because all fingers have the same width.

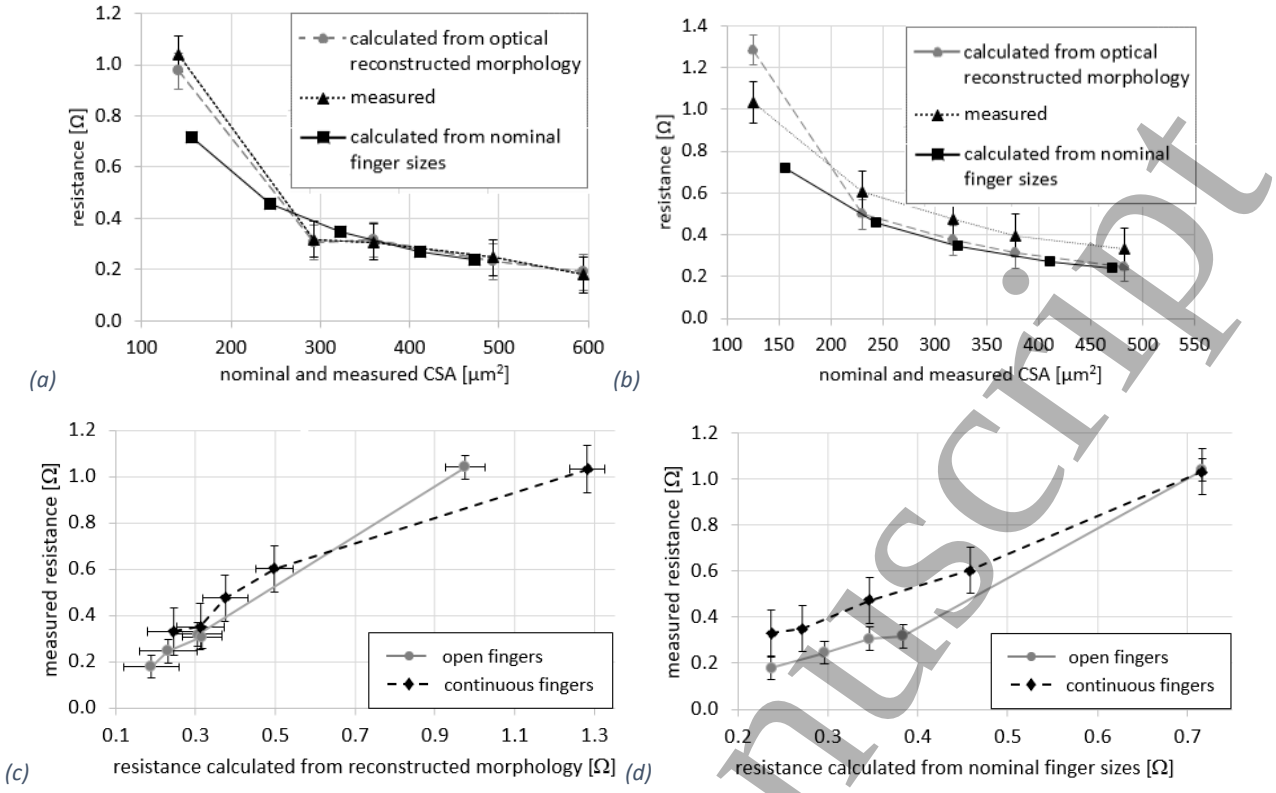

Figure 12 Comparison between measured and calculated resistance on (a) open fingers and (b) fingers connected to the grid on ceramic substrate. Comparison between measured resistance with (c) resistance calculated from reconstructed topography, and with (d) resistance calculated from nominal finger sizes. The error bars refer to standard deviation.

Figure 12 (c) and (d) compare the measured and calculated resistances, namely from optical reconstructed topography and nominal finger sizes. Figure 12 (c) shows a good linear trend for open fingers while more deviations from linearity at different widths are visible for continuous fingers due to the parallel resistance and the approximations of the adopted model. Furthermore, a nearly linear trend between measured resistance and resistance calculated from nominal sizes both for open and continuous fingers, is visible in Figure 12 (d).

Resistance measurements on grid's segments on n-type heterojunction bifacial cells and p-type standard cell are carried out in normal light laboratory conditions. Deviation of results of about 0.5 % – 1 %, well within their expanded uncertainty, were observed in preliminary measurement runs performed in normal light and dark conditions of the laboratory.

As mentioned above, when measuring the resistance of a finger segment, one must distinguish the resistance of the finger itself from those of the other fingers in parallel, and of the silicon substrate. Nevertheless, the influence of the semiconductor itself on the measurements of finger segment resistance is almost negligible by assuming a wafer resistivity of 0.02 Ω·m [23].

A relative expanded uncertainty of 15 % has been estimated for the resistance of segments made by the set-up and the equivalent circuit in Figure 7. A repeatability of about 2.5 % in terms of relative standard uncertainty is achieved by the measurement of the resistances, including probing effects of the finger, while standard uncertainties of less than 1 % each are estimated both for the resistances in parallel by fingers and substrate and for the initial equivalence of finger segments of the same length. A combined standard uncertainty up to 7 % comes both from the terms above and from the resistance measurements (R_{A1} and R_{A2}) at the ends of the segment.

Indeed, for the line resistance calculated by the 3D optical reconstruction of the finger, the relative expanded uncertainty is about 15 %; it takes into account as main contribution the uncertainty of the CSA

mentioned above, while minor contributions are the uncertainties of (i) the segment length, (ii) the resistivity and (iii) thermal effects on the silver paste.

Table 5 Measured and calculated resistances on continuous fingers on ceramic substrate, on central fingers on front and back side of a n-type heterojunction bifacial cell, and on a flawless (position A) and defected (position B) finger segments of the p-type c-Si cell of standard design. The values in brackets refer to standard deviation of measured resistances along the segment.

test cases	***test pattern on alumina***		***heterojunction cell***		***standard c-Si cell***	
segment			*front side*	*back side*	*A*	*B*
nominal width [μm]	*30*	*35*	*32*		*50*	
calculated resistance [Ω]	0.36	0.30	0.63	0.31	0.23	0.27
measured resistance [Ω]	0.47 (0.06)	0.35 (0.04)	0.61 (0.08)	0.28 (0.04)	0.27 (0.04)	-
deviation [%]	23	20	4	10	15	-

In summary, results achieved with standard and bifacial cells and with test patterns on alumina are compared in Table 5. A relative standard deviation within 1 % is obtained by the residuals of a linear fit of the calculated resistance.

With p-type standard c-Si cells, the resistance calculated from the segment morphology differs less than 15 % than the resistance determined on flawless fingers. Due to an interruption along the segment at position B (as identified by the EL image at Figure 3 (b)), comparison with direct resistance are not consistent. A fast way to detect the presence of defects on p-type standard cell grid design, is measuring the resistance between the mid interconnection of pairs of fingers and the busbar nearby. One may clearly observe that possible outlier values are seen in the presence of a defected finger, while closer resistance values are recorded with flawless fingers. The plot in Figure 13 shows the resistance values recorded with the fixed probe on a busbar and the moving probe at contact of nearby mid-interconnections of finger-pairs at position B (Figure 3 (b)). The average amount of such resistance values relates to the mean sizes of fingers of the cell.

Also n-type heterojunction bifacial cells are described by the equivalent circuit in section 3.1.2, thus providing a very low deviation between calculated and measured resistance (Table 5). This confirm that the equivalent circuit and the adopted models represent a rather good approximation of the behaviour of the resistance and 3D morphology of fingers of different sizes and patterns of different design.

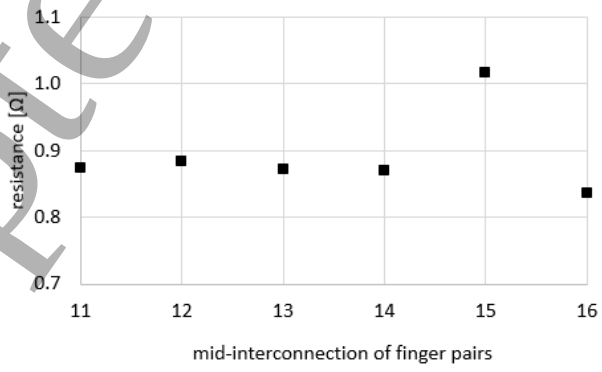

Figure 13 Resistance between the mid-interconnection section of different pairs of fingers and busbar M, at position B, on p-type standard cell.

4. Conclusions

Performances of PV cells in terms of I-V characteristics and efficiency, are tested by standardized methods [31]. Meanwhile, electro- and photo-luminescence (EL, PL) techniques are being introduced for quality control of high-speed production of PLC conductor on PV cells, providing the required sampling capability in terms of lateral resolution and measuring time. EL does not need contacting the cell and is more suitable for fast in-line checks. As a complementary technique, the local optical measurements described above can be performed next-to-line to check the potential local defects, as detected by EL images. Applying the surface-function correlation method described in this work, the resistance can be measured indirectly studying the topography of the electric contact. Furthermore, it is shown that the quality of a printed linear conductor can be easily evaluated through the use of some morphological parameters.

Surface-function correlation is performed for test structures with fingers of 15 µm to 50 µm width and 10 µm to 15 µm thickness deposited on alumina substrate as well as fingers on c-Si PV cell of standard design and on PV bifacial cells. Morphology and resistance measurements of PLC fingers on the test cases are made using a high-resolution confocal microscopy and a 4-wire like set-up.

Morphological characterizations are studied assuming a slightly trapezoidal cross-section shape of fingers, described by the new descriptor CSA. A significant correlation between cross-section-based calculated resistance from 3D reconstructed morphology of fingers and local resistance measurements is achieved with either test structures on alumina and c-Si PV cells. In c-Si p-type and in bifacial solar cells, a relative difference from about 4 % to 15 % between cross-section-based calculated resistance and measured resistance is achieved by assuming a typical resistivity of $2.7 \cdot 10^{-8}$ Ω·m. In ceramic test pattern, the relative difference is about 20 % by assuming a typical resistivity of $2.8 \cdot 10^{-8}$ Ω·m, possibly due to the difference in curing of the grid of these test structures compared to standard inline process. Among others, the presence of local defects of fingers is detected by resistance measurements between busbars and mid-interconnections of pairs of fingers on c-Si PV cell of standard design.

Morphology parameters are extracted from the top finger longitudinal profile, and the spatial wavelength distribution is studied, showing a dominant texture component at about 120 µm - 140 µm in all flawless fingers. Furthermore, the root mean square roughness parameter R_q is calculated for each finger different cut-off lengths (spatial filtered cut-off wavelengths). In general, for short cut-off lengths L, the R_q parameter increases with the sampling length as $R_q \propto L^{\alpha}$. Surfaces may exhibit different scaling at different cut-off ranges. The scaling factor α is given by the slope of the log-log plot of R_q versus the cut-off length L. Moreover, the complexity of the top surface is studied by the calculation of the fractal dimension F, that is in good agreement with the roughness scaling factor according to the relationship $\alpha = 2 - F$. In general, it can be stated that defectless fingers have roughness scaling of about 0.5, F values of about 1.5, R_q roughness values of about 3.3 µm.

Finally, CSA profile along the finger segment is studied in terms of the waviness parameters, in order to quickly identify the presence of defects, interruptions or bottlenecks in the finger and the resistance behaviour of fingers. The measurements performed show a total waviness peak parameter $W_A t$ of about 12 µm², $W_A sk$ with positive values, indicating a low presence of valleys in the waviness profile (and so a low presence of interruption and/or bottleckness), and $W_A ku$ is always greater than 3, except for thinner fingers that present inhomogeneities.

5. Glossary

2D: bidimensional
3D: three-dimensional
α: rms roughness scaling factor
θ_f: finger side slope
λ_c: high-pass cut-off value of roughness profile
λ_f: high-pass cut-off value of waviness profile
ρ_f: gridline resistivity of the silver paste
c-Si: crystalline silicon

CSA: trapezoidal calculated cross-section area
dl: elementary segment length
EL: electroluminescence
F: fractal dimension
GPS: geometrical product specification
INRiM: Istituto Nazionale di Ricerca Metrologica
L: cut-off length (spatial filtered cut-off wavelength)
PLC: printed linear conductor
PV: photovoltaic
PL: photoluminescence
PSI: phase-shifting interferometry
rms: root-mean-square
R_a: average of the roughness profile
R_q: rms of the roughness profile
R_z: maximum height of the roughness profile
R_At: maximum height of CSA profile
R_A: resistance in the finger segment L_A
R_B: resistance in the finger segment L_B
R_C: parallel resistance
R_S: series resistance
R: line resistance calculated in the segment length analysed $1-2$
R_1: resistance measured in the point 1
R_2: resistance measured in the point 2
R_{A1}: resistance measured without the influence of the grid parallel and the series resistance in the point 1
R_{A2}: resistance measured without the influence of the grid parallel and the series resistance in the point 2
R_i: resistance of the elementary segment calculated by the second Ohm law
SS: structured surfaces
st. dev.: standard deviation
TCO: transparent conductive oxide
t_f: finger thickness
USSF: universal substrate sample fixture
VSI: vertical scanning interferometry
W_f: finger width
W_p: maximum peak height of waviness profile
W_v: maximum valley depth of waviness profile
W_At: total height of cross-section area waviness profile
W_Ask: skewness of cross-section area waviness profile
W_Aku: kurtosis of cross-section area waviness profile

Acknowledgments

The parent project 14 IND 09 MetHPM is delivered under the EMPIR initiative, which is co-funded by the EU's Horizon 2020 research and innovation programme and the EMPIR Participating States.

ORCID iDs

Gian Bartolo Picotto, https://orcid.org/0000-0002-7014-0629
Luigi Ribotta, https://orcid.org/0000-0001-5334-5246

References

[1] W. P. Dong, P. J. Sullivan, K. J. Stout, Comprehensive study of parameters for characterising three-dimensional surface topography III: Parameters for characterising amplitude and some functional properties, *Wear*, 178, 1994, 29-43
[2] M. Galiazzo, A. Voltan, M. Bertazzo, W. Tao, X. Zhang, J. Shi, D. Zhang, Z. Hu, J. Wang, Extensive comparison of solar modules manufactured with single and double printed cells, *Energy Procedia*, 2015, 77, 520-526
[3] International Technology Roadmap for Photovoltaic ITRPV 9th edition 2018 – report release and key findings, Markus Fischer, PV CellTech Conference, March 14 2018, Penang, Malaysa, https://www.pvmen.com/upload/attachment/201803/20/053037/ITRPV%20Ninth%20Edition%20Presentation%202018.pdf, web access June 2019

[4] M. Galiazzo, A. Voltan, E. Bortoletto, M. Zamuner, M. Martire, O. Borsato, M. Bertazzo, D. Tonini, Fine Line Double Printing and Advanced Process Control for Cell Manufacturing, *Energy Procedia*, 2015, 67, 116-125
[5] L. Serenelli, M. Izzi, R. Chierchia, E. Salza, P. Mangiapane, M. Tucci, *Screen printing a bassa temperatura di sintering a bassa resistività specifica di contatto sia su ITO che su AZO*, ENEA and Italian Ministry of Economic Development, 2013
[6] C. Zhai, D. Hanaora, G. Proust, L. Brassart, Y. Gan, Interfacial electro-mechanical behaviour at rough surfaces, *Extreme Mechanics Letters* 9 (2016) 422–429
[7] K. Ryu, Y. Moon, K. Park, J-Y Hwang, S-J Moon, Electrical Property and Surface Morphology of Silver Nanoparticles After Thermal Sintering, *Journal of Electronic Materials*, 45, 1, 2016
[8] R. Tala-Ighil, F. Chelli, S. Sali, S. Oussalah, M. Boumaour, F. Tayour, Y. Si-Ahmed, Electrical and morphological study of screen printed silicon solar cells contacts, *Archives Des Sciences*, 65, 10, 2012
[9] L. Jiang, W. Zhang, T.Guo, D.Kapp, L. Yan, L. Wang, An improved mathematical modelling to simulate metallization screen pattern trend for silicon solar cell, *Photovoltaic Specialists Conference (PVSC) 2013 IEEE 39th*, 2013, 2641-2645
[10] R. Leach, C. Evans, L. He, A. Davies, A. Duparré, A. Henning, C. W. Jones, D. O'Connor, Open questions in surface topography measurement: a roadmap, *Surf. Topogr.: Metrol. Prop*. 3 (2015) 013001
[11] L. De Chiffre, P. Lonardo, H. Trumpold, D. A. Lucca, G. Goch, C. A. Brown, J. B. Raja, H. N. Hansen, Quantitative Characterisation of Surface Texture, CIRP Annals, 49, 2, 2000, 635-642
[12] ISO/DIS 25178-607 Geometrical product specifications (GPS)—Surface texture: areal—Part 607: Nominal characteristics of non-contact (confocal microscopy) instruments, International Organization for Standardization, Geneva, 2017 (www.iso.org/obp/ui/#iso:std:iso:25178:-607:dis:ed-1:v1:en), web access March 2019
[13] ISO 4287:1997 Geometrical Product Specifications (GPS) -- Surface texture: Profile method -- Terms, definitions and surface texture parameters, Geneva: International Organization for Standardization, Geneva, (www.iso.org/standard/10132.html) , web access March 2019
[14] ISO 5436-1:2000, Geometrical Product Specifications (GPS) -- Surface texture: Profile method; Measurement standards -- Part 1: Material measures, Geneva: International Organization for Standardization (https://www.iso.org/standard/21978.html), web access March 2019
[15] Metrology for Highly-Parallel Manufacturing MetHPM, EMPIR 14IND09 project, website http://empir.npl.co.uk/methpm/project/, web access January 2019
[16] DigitalSurf MountainsMap 7 Premium, website http://www.digitalsurf.com/en/mntpremium.html, web access February 2019
[17] Image Metrology SPIP, website https://www.imagemet.com/products/spip/, web access February 2019
[18] C. W. Jones, M. Santiano, S. Downes, R. Bellotti, D. O'Connor, G. B. Picotto, A universal substrate sample fixture for efficient multi-instrument inspection of large, flexible substrates, with absolute position registration support, Proc. euspen 16th Intl. Conf., Nottingham UK, 30 May – 3 June 2016
[19] Keysight 3458A Multimeter User's Guide, Agilent Technologies, 2014
[20] NIST Engineering Metrology Toolbox (http://emtoolbox.nist.gov/Main/Main.asp), web access January 2019
[21] C. Zhai, D. Hanaor, G. Proust, Y. Gan, Stress-Dependent Electrical Contact Resistance at Fractal Rough Surfaces, *Journal of Engineering Mechanics*, 2015, 143(3):B4015001
[22] R. Bellotti, V. Furin, C. Maras, G. B. Picotto, L. Ribotta, A function-driven characterization of printed conductors on PV cells, *Surf. Topogr.: Metrol. Prop*. 6 (2018) 025002
[23] H. Hannebauer, T. Dullweber, T. Falcon, R. Brendel, Fineline printing options for high efficiencies and low Ag paste consumption, *Energy Procedia*, 2013, 38, 725-731
[24] A guide to roundness & surface texture, Taylor Hobson, UK, 2017
[25] ISO 4288:1996, Geometrical Product Specifications (GPS) -- Surface texture: Profile method -- Rules and procedures for the assessment of surface texture, Geneva: International Organization for Standardization, Geneva, (https://www.iso.org/standard/2096.html), web access March 2019
[26] S. Talu, S. Stach, M. Ikram, D. Pathak, T. Wagner, J-M Nunzi, Surface Roughness Characterization of ZnO: TiO_2-Organic Blended Solar Cells Layers by Atomic Force Microscopy and Fractal Analysis, International Journal of Nanoscience, 13, 3 (2014) 1450020
[27] C.-C. Chou, H.-H. Lin, Fractal dimension and surface topography on the diamond deposition of seeded WC–Co substrates, *Journal of Applied Physics*, 2010, 107 (7), 073510
[28] B. Raabe, F. Huster, M. McCann, P. Fath, High Aspect Ratio screen printed fingers, *20th European Photovoltaic Solar Energy Conference, Proceedings of the International Conference*, Barcelona, ES, 6-10 June, 2005, ISBN:3-936338-19-1
[29] Introduction to roughness, Keyence, https://www.keyence.com/ss/products/microscope/roughness/index.jsp, web access February 2019
[30] M. Aoki, K. Nakamura, T. Tachibana, I. Sumita, H. Hayashi, H. Asada, Y. Ohshita, 30μm Fine-Line Printing for Solar Cells, *Conference Record of the IEEE Photovoltaic Specialists Conference*, 2013, DOI: 10.1109/PVSC.2013.6744903
[31] IEC TS 60904:2018, Photovoltaic devices, International Electrotechnical Commission, https://webstore.iec.ch/publication/3881, web access March 2019